Pseudopotentials for an ultracold dipolar gas

T.M. Whitehead[1] and G.J. Conduit[1]

[1] *Cavendish Laboratory, J.J. Thomson Avenue, Cambridge, CB3 0HE, United Kingdom*

(Dated: January 25, 2016)

A gas of ultracold molecules interacting via the long-range dipolar potential offers a highly controlled environment in which to study strongly correlated phases. However, at particle coalescence the divergent $1/r^3$ dipolar potential and associated pathological wavefunction hinder computational analysis. For a dipolar gas constrained to two dimensions we overcome these numerical difficulties by proposing a pseudopotential that is explicitly smooth at particle coalescence, resulting in a 2000-times speedup in diffusion Monte Carlo calculations. The pseudopotential delivers the scattering phase shifts of the dipolar interaction with an accuracy of 10^{-5} and predicts the energy of a dipolar gas to an accuracy of $10^{-4}E_{\mathrm{F}}$ in a diffusion Monte Carlo calculation.

I. INTRODUCTION

Ultracold atomic gases are an ideal testing ground for many-body quantum physics. Experiments now allow the condensation of particles that carry either an electric or magnetic dipole moment, and so interact through the long-ranged dipolar interaction in a highly controlled environment [1–10]. These systems present an ideal opportunity to study emergent strongly correlated phenomena driven by long-range interactions [11–21]. However, numerical studies of the dipolar interaction are complicated by the pathological behavior of the wavefunction at particle coalescence. We propose a pseudopotential for the dipolar interaction that delivers almost identical scattering properties to the original dipolar interaction, but has a smooth profile that accelerates diffusion Monte Carlo calculations by a factor of ~ 2000.

In recent years there have been rapid developments in forming, trapping, and cooling ultracold atoms and molecules with dipole moments. These experiments have involved fermionic [1] or bosonic [2] particles with magnetic [3] or electric [4] dipole moments, in the continuum [11] or a lattice potential [22]. For the sake of concreteness we consider a gas of fermionic dipolar particles [1, 5, 6]. A particularly appealing geometry is a single component gas of fermions trapped in two dimensions [10]. This configuration can suppress the chemical reaction rate of the molecules, thereby giving sufficient time to relax and study strongly correlated phases [23], and a strong external field can align the dipoles at an angle θ to the normal to the plane, which allows fine control over the interactions between the particles. The dipolar interaction between the particles is then $V(r,\phi) = d^2[1 - \frac{3}{2}\sin^2\theta(1+\cos 2\phi)]/r^3$ where ϕ is the polar angle in the plane, measured from the projection of the electric field onto the plane, r is the interparticle distance, and d is the dipole moment. We focus on the fully repulsive regime of the potential, with $\theta \leq \theta_{\mathrm{c}} = \arcsin(1/\sqrt{3})$, where there are no bound states. In the special case $\theta = 0$ the potential $V(r,\phi)$ reduces to the isotropic form $V(r) = d^2/r^3$.

Theoretical studies of the dipolar gas have provided a rich variety of surprises and insights. Remarkably, even at mean-field level the non-tilted ($\theta = 0$) system with an isotropic potential is predicted to display an inhomogeneous stripe phase [24, 25] that is robust to the inclusion of perturbative quantum fluctuations [13]. To extend beyond the perturbative regime theorists have turned to diffusion Monte Carlo [26]: however, the divergent dipolar potential and associated pathological wavefunction make these simulations difficult to carry out, and they have not uncovered evidence of the exotic inhomogeneous stripe phase.

The disagreement between analytical and numerical studies motivates us to focus our efforts on improving the modeling of the troublesome dipolar potential. Similar difficulties with divergent potentials arise in the study of the contact and Coulomb interactions, where it has been shown that pseudopotentials can accurately mimic the real interaction [27, 28]. We follow the same prescription to now construct a pseudopotential that delivers the same scattering physics as the dipolar interaction, but which is smooth at particle coalescence and so avoids the numerical difficulties arising from pathological behavior near particle coalescence.

This smoothness will provide benefits in a variety of numerical techniques, including configuration interaction methods [29], coupled cluster theory [30], and diffusion Monte Carlo (DMC) [31]. Here we analyze the performance of the pseudopotential by carrying out DMC calculations on the dipolar gas to find the ground state energy of the system. We find that the proposed pseudopotential delivers ground state energies with an accuracy of order $10^{-4}E_{\mathrm{F}}$, whilst also offering a speedup by a factor of ~ 2000 relative to using the dipolar potential.

We start by studying the two-body scattering problem. In Section II we analytically solve the wavefunction of the non-tilted $\theta = 0$ system near to particle coalescence, which offers insights into the numerical difficulties. Building on the analytical solution, in Section III we numerically solve the two-body problem of scattering from the dipolar potential out to larger radii. This provides the scattering phase shift that we use to calibrate the scattering from the pseudopotential. Having proposed the pseudopotential, in Section IV we test it on a second two-body system: two particles in a parabolic

trap. In Section V we then demonstrate the use of the pseudopotential to study the ground state energy of the many-body fermionic gas, confirming both the accuracy of the pseudopotential and the computational speedup. In Section VI we repeat the procedure with tilted dipoles, and in Section VII discuss future applications of the pseudopotential.

II. KATO-LIKE CUSP CONDITIONS

To develop a pseudopotential for the dipolar interaction we need to properly understand scattering from the original dipole. Working with non-tilted dipoles, we focus on the small radius limit where we can solve for the wavefunction analytically. This will allow us to demonstrate the pathological behavior of the wavefunction and resultant numerical difficulties, and provide boundary conditions for the full numerical solution of the scattering properties. Moreover we will calculate a Kato-like cusp condition, a scheme to partially alleviate these numerical difficulties for the true dipolar potential.

To study the small radius behavior we focus on the two-body problem: two identical same-spin fermions of mass m in their center-of-mass frame with energy $E \geq 0$. The Hamiltonian in atomic units ($\hbar = m = 1$) is

$$\hat{H}\psi(r,\phi) = -\nabla^2\psi(r,\phi) + V(\hat{r})\psi(r,\phi) = E\psi(r,\phi), \quad (1)$$

where $V(r) = d^2/r^3$ is the isotropic dipolar interaction for particle separation r and dipole strength d, with characteristic length scale $r_0 = d^2$.

A key quantity for Monte Carlo methods is the local energy, $E_\mathrm{L} = \psi^{-1}\hat{H}\psi$ [32]. For an eigenstate the local energy is constant, and equal to the eigenenergy, whilst for other wavefunctions the local energy varies in space. The foundation of the many-body trial wavefunction in our Monte Carlo calculations is a non-interacting wavefunction given by a Slater determinant of plane wave states. As two particles approach coalescence their contribution to the wavefunction in each angular momentum channel ℓ is $\psi_{\mathrm{non-int},\ell}(r,\phi) = r^\ell \cos(\ell\phi)$, which is an eigenstate of the two-body non-interacting system. The Slater determinant gives such a contribution in every odd angular momentum channel. In Fig. 1 we demonstrate that when this wavefunction is used with the dipolar potential the local energy diverges as r^{-3} in every angular momentum channel. This divergence is unwelcome as it will make the local energy difficult to sample in Monte Carlo calculations, and the variance of the samples will give rise to a large statistical uncertainty in the calculated energy.

To try to remedy this divergence in the local energy we examine the exact eigenstates of the two-body Hamiltonian given by Equation (1), and then apply our findings to the many-body system. In the small separation limit where the potential $V(r)$ diverges the eigenstates of the Hamiltonian are

$$\psi_\ell(r,\phi) = K_{2\ell}(2\sqrt{r_0/r})\cos(\ell\phi),$$

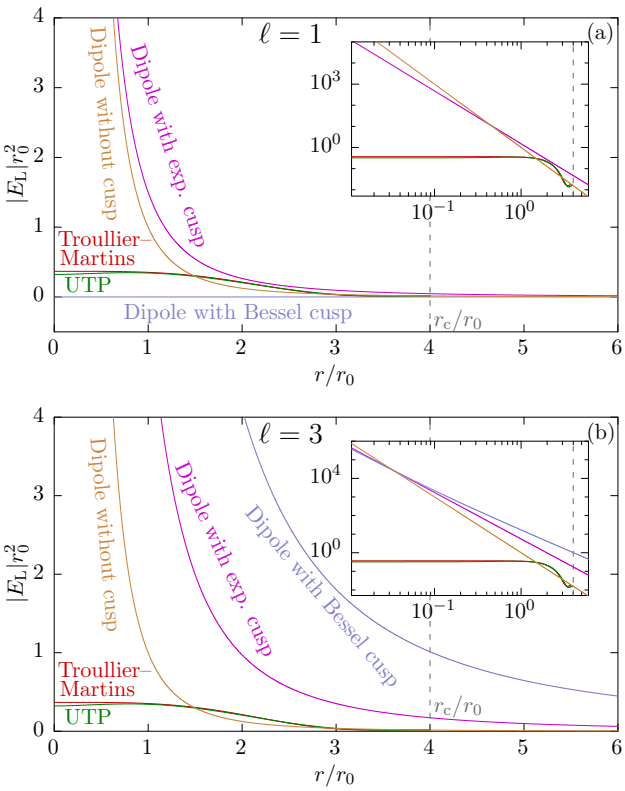

FIG. 1. (Color online) (a) The local energy $E_\mathrm{L} = \psi^{-1}\hat{H}\psi$ as a function of radius in the $\ell = 1$ angular momentum channel, showing in orange the divergence as r^{-3} when the dipolar potential is used with the non-interacting wavefunction $\psi_{\mathrm{non-int},\ell=1}$. Also shown in magenta is the local energy divergence as $r^{-5/2}$ when the dipolar potential is used with a wavefunction with an exponential cusp correction $\psi_{\mathrm{exp},\ell=1}$, and in blue the exact solution in this channel, given by a Bessel function cusp correction $\psi_{K_2,\ell=1}$. In red and green are the local energies of Troullier–Martins and ultratransferable (UTP) pseudopotentials, respectively, with the non-interacting wavefunction, which outside of the radius r_c shown by a dashed gray line join smoothly onto the real dipolar potential. The inset shows the same curves on a logarithmic scale. (b) The local energy in the $\ell = 3$ channel, demonstrating that the Bessel function cusp correction $\psi_{K_2,\ell=3}$ is not accurate in other channels.

where $K_n(x)$ is a modified Bessel function of the second kind and the quantum number ℓ denotes angular momentum projected onto the polar axis. In order to turn the $\ell = 1$ part of the non-interacting wavefunction given by the Slater determinant into an eigenstate of the Hamiltonian with the dipolar interaction we may multiply the Slater determinant by a factor $K_2(2\sqrt{r_0/r})/r$, which we refer to as a Bessel function cusp correction. This gives a wavefunction that is a zero-energy eigenstate of the Hamiltonian in the $\ell = 1$ channel, as shown in Fig. 1(a). Similar Bessel function cusp corrections have been used previously to study both fermionic and bosonic systems [14, 19, 26].

In Monte Carlo calculations we have to pre-multiply

the entire Slater determinant, and so all angular momentum channels present in it, by a single cusp correction term, and it is not practical to adapt the cusp correction on the fly to the relative angular momentum of interacting particles. However, the Bessel function cusp correction applied to the two-body wavefunction,

$$\psi_{K_2,\ell}(r,\phi) = r^\ell \cos(\ell\phi) K_2(2\sqrt{r_0/r})/r,$$

is not an eigenstate in any angular momentum channel except $\ell = 1$. In other channels it gives a local energy that diverges as $r^{-5/2}$ in the $r \to 0$ limit, as shown in Fig. 1(b) for the $\ell = 3$ channel.

The improvement of the divergence in the local energy from r^{-3} to $r^{-5/2}$ is, in fact, due to the leading-order behavior of the Bessel function cusp correction, which goes as $\exp(-2\sqrt{r_0/r})$, independent of angular momentum. Accepting that we will always be left with an $r^{-5/2}$ divergence of the local energy in many-body calculations, we may then just take this leading order term to give an exponential cusp correction, leading to a wavefunction

$$\psi_{\mathrm{exp},\ell}(r,\phi) = r^\ell \cos(\ell\phi) \exp(-2\sqrt{r_0/r}).$$

The $r^{-5/2}$ divergence of the local energy with this wavefunction is shown in Fig. 1 for angular momentum channels $\ell = 1$ and $\ell = 3$.

The approach of inserting a small radius analytical solution into the many-body trial wavefunction is well established in electronic-structure calculations where the small radius behavior of the wavefunction around the $1/r$ divergence in the Coulomb potential is fixed with the Kato cusp conditions [33, 34]. Following this prescription we can premultiply a many-body non-interacting trial wavefunction by the exponential cusp correction $\prod_{i>j} \exp(-2\sqrt{r_0/r_{ij}})$ or Bessel function cusp correction $\prod_{i>j} K_{2\ell}(2\sqrt{r_0/r_{ij}})/r_{ij}^\ell$, where the product is over all dipoles labeled by i, j and r_{ij} is the dipole-dipole separation. Similarly to the two-body case both corrections leave an $r^{-5/2}$ divergence in the local energy, which will manifest itself as a major contribution to the uncertainty in the final prediction of the energy. We will revisit the question of cusp corrections in a many-body system in Fig. 5(b), where we show that the simple exponential cusp correction gives similar values for the variance in the local energy to a full Bessel function cusp correction.

In order to study the interacting-dipole system further we turn to the construction of pseudopotentials [27, 35] that capture the physics of the system whilst delivering the smooth and non-divergent local energy values shown in Fig. 1.

III. DERIVATION OF THE PSEUDOPOTENTIALS

To construct a pseudopotential for the dipolar interaction we continue with the two-body scattering problem of two indistinguishable fermions in their center-of-mass frame, studying the Schrödinger Equation (1). We seek a pseudopotential that is smooth and non-divergent to accelerate numerical calculations. We also require it to reproduce the correct two-body scattering physics over the range of scattering energies present in a Fermi gas with Fermi energy E_F, which guarantees that the pseudopotential will properly capture two-body effects in the system. As we will be considering two-body processes we again work in the center-of-mass frame, with the Hamiltonian given by Equation (1).

We first turn to the Troullier–Martins [35] formalism that has been widely used and rigorously tested in the literature to construct attractive electron-ion pseudopotentials [36–41], but which may be adapted [27] to the current problem of two identical fermions as detailed in Appendix A. This method creates a pseudopotential with the exact dipolar potential outside of a cutoff radius r_c and a polynomial potential within it, constructed to be smooth up to second derivative at r_c. The Troullier–Martins method guarantees that the scattering properties of the pseudopotential will be exact at one particular calibration energy E_c. We choose the calibration energy to be the average scattering energy of two fermions in a non-interacting Fermi gas. In Appendix B we show that this calibration energy is $E_\mathrm{c} = E_\mathrm{F}/4$.

For the scattering of two indistinguishable fermions the Pauli principle guarantees that there will be no s-wave contribution to the scattering. We therefore construct the Troullier–Martins pseudopotential by focusing on a scattering wavefunction in the p-wave, $\ell = 1$, channel. The functional form of the pseudo-wavefunction in this channel is

$$\psi_{\ell=1}(r,\phi) = \begin{cases} \exp[p(r)]\, r\cos(\phi)\,, & r < r_\mathrm{c}\,, \\ \psi_{\mathrm{dipole},\ell=1}(r,\phi)\,, & r \geq r_\mathrm{c}\,, \end{cases} \tag{2}$$

where the polynomial $p(r) = \sum_{i=0}^{6} c_i r^{2i}$, and the wavefunction $\psi_{\mathrm{dipole},\ell=1}(r,\phi)$ is calculated by numerically solving Equation (1) using the exact dipolar potential at the calibration energy E_c. As explained in Appendix A the coefficients c_i are calculated by requiring continuity of the pseudo-wavefunction and its first four derivatives at r_c, as well as matching the net density inside r_c, and requiring the pseudopotential to have zero gradient and curvature at the origin.

The choice of r_c is motivated by the physics we wish to study: a longer cutoff radius allows a smoother potential that gives efficient numerics, but being less similar to the real potential has less accurate phase shift errors. In many-body systems the longer cutoff radius will also increase the probability of having three or more particles within the cutoff radius, which the pseudopotential is not designed to be able to accurately model. For our two-body scattering system we take $k_\mathrm{F} r_\mathrm{c} = 2$.

The exponentiated polynomial form of the pseudo-wavefunction in Equation (2) means that the Schrödinger Equation (1) may be analytically inverted to give the

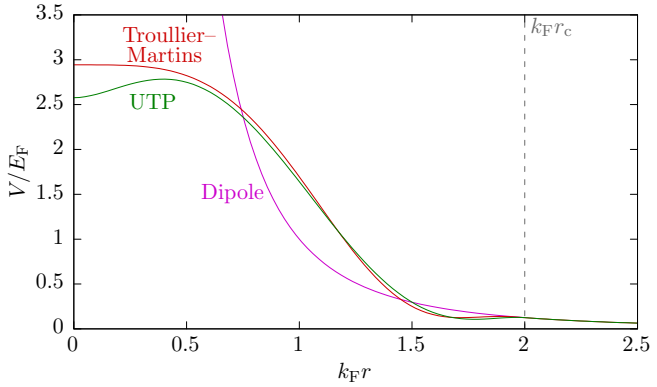

FIG. 2. (Color online) The dipolar potential, and Troullier–Martins and UTP pseudopotentials. The gray vertical line indicates r_c, the pseudopotential cutoff radius.

pseudopotential as

$$V_{\text{T–M}}(r) = \begin{cases} E_c + \frac{3}{r}p' + p'^2 + p'', & r < r_c\,, \\ d^2/r^3\,, & r \geq r_c, \end{cases} \quad (3)$$

where the primes denote differentiation with respect to r. This pseudopotential is shown in red in Fig. 2 for interaction strength $k_F r_0 = 1/2$. It is non-divergent at particle coalescence and smooth where it joins onto the real dipolar potential at $r = r_c$. This pseudopotential gives rise to the local energy E_L shown in Fig. 1. The smooth and finite local energy at $r < r_c$ is a dramatic improvement over the divergent local energy from our trial wavefunction with the dipolar potential, and this non-divergence should lead to improved statistics and efficiency in many-body simulations.

To measure the accuracy of our pseudopotentials we calculate the phase shift in the wavefunction

$$\delta_{\psi,\ell}(E) = \frac{1}{2\pi}\text{arccot}\left[\frac{1}{\sqrt{E}}\left(\frac{\psi'_\ell(r_c,\phi)}{\psi_\ell(r_c,\phi)} + \frac{2\ell+1}{2r_c}\right)\right] \quad (4)$$

imparted by a two-body scattering process, where $\delta_{\psi,\ell}$ is evaluated at the cutoff radius r_c because any difference in phase shift must be accumulated in the region $r < r_c$ where the potentials differ. The difference between the scattering phase shift for the Troullier–Martins pseudopotential and the exact phase shift from the dipolar interaction is shown in red in Fig. 3(a) as a function of scattering energy, evaluated at $k_F r_0 = 1/2$. The scattering phase shift of the Troullier–Martins pseudopotential is exact at the calibration energy, and accurate to order 10^{-5} over the range of scattering energies in a Fermi sea.

Although the Troullier–Martins pseudopotential captures the exact scattering properties at the calibration energy, it deviates at all other energies, with the leading order deviation around the calibration energy going as $(E - E_c)^2$ [27]. A natural extension to the Troullier–Martins formalism is to find a pseudopotential that minimizes this deviation in the phase shift over all the possible

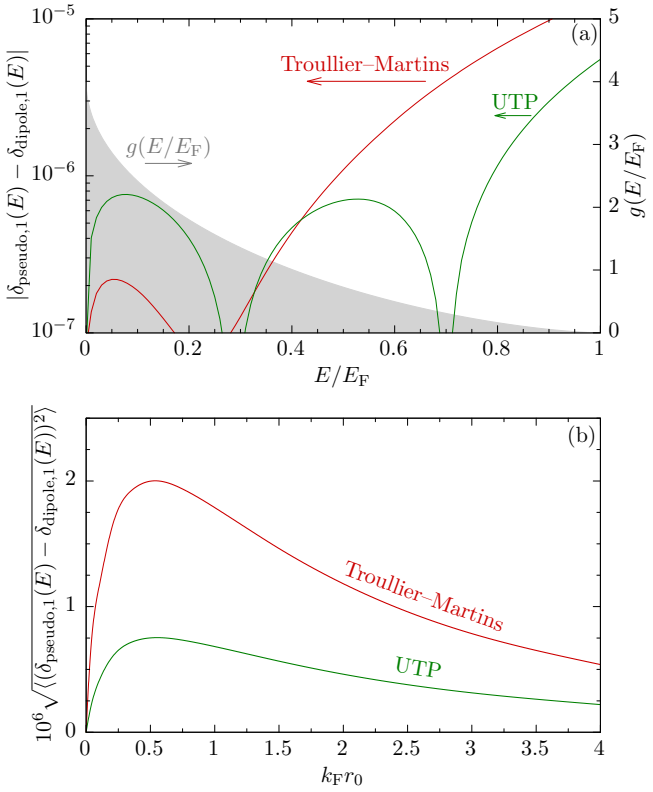

FIG. 3. (Color online) (a) The error in the scattering phase shift $|\delta_{\text{pseudo},1}(E) - \delta_{\text{dipole},1}(E)|$. The filled gray curve is the density of scattering states $g(E)$ in the two-body Fermi sea on a linear scale. (b) The root-mean-squared error in the scattering phase shift as a function of interaction strength.

relative energies of pairs of particles in a Fermi gas. We derive such a pseudopotential here, referring to it as an "ultratransferable pseudopotential" (UTP).

The UTP [27] is identical to the dipolar potential outside a cutoff radius r_c, but has a polynomial form inside the cutoff,

$$V_{\text{UTP}}(r) = \frac{d^2}{r_c^3}\begin{cases} 1 + 3\left(1 - \frac{r}{r_c}\right)\left(\frac{r}{r_c}\right)^2 + \\ \left(1 - \frac{r}{r_c}\right)^2\left[v_1\left(\frac{1}{2} + \frac{r}{r_c}\right) + \sum_{i=2}^{N_v} v_i\left(\frac{r}{r_c}\right)^i\right], & r < r_c\,, \\ r_c^3/r^3\,, & r \geq r_c, \end{cases}$$

with $N_v = 3$. The term $1 + 3(1 - r/r_c)(r/r_c)^2$ guarantees that the potential and its first derivative are continuous at $r = r_c$. In the next term, the expression $(1 - r/r_c)^2$ also ensures continuity of the potential at the cutoff radius, and $v_1(1/2 + r/r_c)$ constrains the potential to have zero derivative at the origin. This ensures that the pseudo-wavefunction is smooth, easing the application of numerical methods.

To determine the coefficients $\{v_i\}$ we minimize the total squared error in the phase shift over all the possible

pairs of interacting particles in a Fermi gas

$$\left\langle \left|\delta_{\mathrm{UTP},\ell}\left(E\right)-\delta_{\mathrm{dipole},\ell}\left(E\right)\right|^2\right\rangle = \int \left|\delta_{\mathrm{UTP},\ell}\left(E\right)-\delta_{\mathrm{dipole},\ell}\left(E\right)\right|^2 g(E/E_{\mathrm{F}})\,\mathrm{d}E/E_{\mathrm{F}}\,, \quad (5)$$

where

$$g(x) = 4 - \frac{8}{\pi}\left(\sqrt{x(1-x)} + \arcsin\sqrt{x}\right)$$

is the density of scattering states in energy (see Appendix B and Reference [42]), shown in Fig. 3(a). The density of scattering states decreases as a function of energy due to the finite size of the Fermi sea of scattering particles limiting the available range of scattering energies. We primarily work in the leading-order $\ell = 1$ angular momentum channel. The UTP formalism is capable of creating pseudopotentials that are accurate in several angular momentum channels by summing over them in Equation (5) whilst accounting for the occupation of the channels that goes as $1/\sqrt{(2\ell+1)!!}$ [28], which strongly suppresses the effect of all the channels above $\ell = 1$. The total squared phase shift error Equation (5) is numerically minimized with respect to the v_i to create our UTP.

The scattering phase shift behavior of the UTP is shown in Fig. 3(a). Although it is less accurate than the Troullier–Martins pseudopotential at the Troullier–Martins calibration energy, the UTP is more accurate at higher incident energies. At zero scattering energy both pseudopotentials are exact, as the scattering particles never penetrate the region $r < r_{\mathrm{c}}$ where the pseudopotentials deviate from the real dipolar interaction.

In Fig. 3(b) we show the average phase shift error in the pseudopotentials as a function of interaction strength. At its worst the Troullier–Martins pseudopotential has an average accuracy of 2×10^{-6}, whilst the average UTP accuracy is always better than 1×10^{-6}. Over a broad range of interaction strengths the UTP is more accurate than the Troullier–Martins pseudopotential, but both are exact at $k_{\mathrm{F}} r_0 = 0$ where the particles do not interact. At high interaction strengths the pseudopotentials become highly accurate, as the increasing interaction strength effectively rescales the potential size, and so for a given range of scattering energies the particles will be kept further apart and so less strongly probe the region $r < r_{\mathrm{c}}$ where the potentials differ. We also note that a further advantage of the UTP is that at high interaction strengths, $k_{\mathrm{F}} r_0 > 4$ with $k_{\mathrm{F}} r_{\mathrm{c}} = 2$, it is not possible to solve the system of equations defining the Troullier–Martins pseudopotential, whilst it is still possible to derive a UTP.

Having constructed two different pseudopotentials and demonstrated their accuracy in a homogeneous two-body setting, we now test their flexibility by solving an inhomogeneous two-body system.

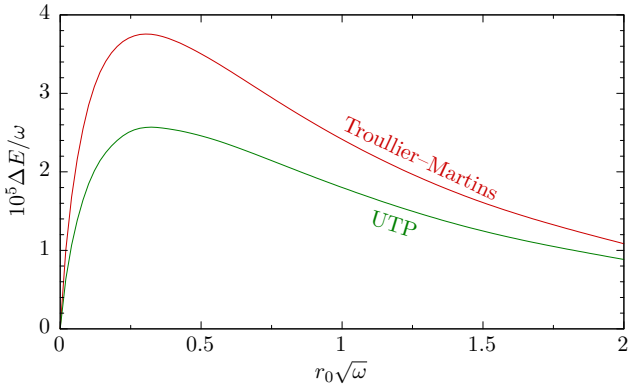

FIG. 4. (Color online) The deviation of the energy of two particles in an harmonic trap as calculated using both Troullier–Martins and UTP pseudopotentials from that calculated using the exact dipolar potential, as a function of interaction strength.

IV. TWO FERMIONS IN AN HARMONIC TRAP

We have developed pseudopotentials that exhibit the correct scattering properties for an isolated two-body system. To test them we turn to the experimentally realizable [43, 44] configuration of two fermionic dipolar particles aligned by an external field and held in a circularly symmetric two-dimensional harmonic well with trapping frequency ω. Given that the identical fermions must be in different single-particle states of the harmonic trap the non-interacting energy of the reduced system is 2ω. This system is a good place to test our pseudopotentials as it has a non-trivial background potential, but at the same time is still simple enough to solve accurately with the real dipolar potential.

We calculate the energy of two particles held in such a trap by solving the Schrödinger equation for the relative motion in the system,

$$-\nabla^2\psi + \frac{1}{4}\omega^2 r^2 \psi + V(r)\psi = E\psi\,, \quad (6)$$

with $V(r)$ set as either the exact dipolar potential or a pseudopotential. We solve the system in the lowest-energy $\ell = 1$ angular momentum channel available to identical fermions, calibrating the Troullier–Martins pseudopotential at $E_{\mathrm{c}} = (2\omega)/4 = \omega/2$ by analogy to the homogeneous system. For the cutoff radius r_{c} we choose the characteristic width of the trap, $1/\sqrt{\omega}$.

The energy differences between the pseudopotential and exact dipolar solutions to Equation (6) are shown in Fig. 4 as a function of interaction strength. Approaching zero interaction strength the form of the interaction potential has diminishing impact, and so the difference in energies goes to zero; and in the high-interaction strength limit the particles are kept further apart by the strong potential, so less strongly probe $r < r_{\mathrm{c}}$ where the potentials differ and again the error in the ground state

energy becomes negligible. At intermediate interaction strengths $r_0\sqrt{\omega} \approx 1/4$ the pseudopotentials are still accurate to order $10^{-5}\omega$, which exceeds the $\sim 10^{-4}\omega$ accuracy attainable in exact diagonalization [45] and many-body quantum Monte Carlo calculations [26, 27, 46]. The UTP provides an improvement in accuracy over the Troullier–Martins pseudopotential at all interaction strengths.

V. FERMI GAS

Having demonstrated that the Troullier–Martins and UTP pseudopotentials are accurate tools for studying both scattering and inhomogeneous trapped two-body systems, we are well placed to test the pseudopotentials in a many-body system: a gas of fermionic dipolar particles. The particles are constrained to lie in two dimensions with all their dipole moments aligned normal to the plane, which has been suggested for experimental investigation [10]. We use diffusion Monte Carlo (DMC) calculations to study the system, using the CASINO code [32].

A. Formalism

Our DMC calculations use 81 particles per simulation cell and a Slater–Jastrow type wavefunction $\Psi = \mathrm{e}^J D$. Here D is a Slater determinant of plane-wave orbitals, with wavevectors given by the reciprocal lattice vectors of our simulation cell, and the Jastrow factor e^J describes the interparticle correlations [47], with

$$J = \sum_{i\neq j}\left(\sum_{k=0}^{N_\mathrm{u}} u_k r_{ij}^k \left(1-\frac{r_{ij}}{L}\right)^3 \Theta\left(L-r_{ij}\right) + \sum_{\mathbf{G}} p_{|\mathbf{G}|}\cos(\mathbf{G}\cdot\mathbf{r}_{ij})\right), \tag{7}$$

where the first sum runs over all particles labeled i, j with separation $\mathbf{r}_{ij}$, $N_\mathrm{u} = 7$, and the $\mathbf{G}$ vectors are the 36 shortest reciprocal lattice vectors (first 8 sets of equal-length reciprocal lattice vectors). The cutoff function $(1 - r_{ij}/L)^3$ ensures that the wavefunction's first two derivatives go smoothly to zero at a radius L, chosen to be the Wigner-Seitz radius of the simulation cell. Calculations with the exact dipolar interaction have a cusp correction term in the Jastrow factor, using the exponential form $\prod_{i>j}\exp(-2\sqrt{r_0/r_{ij}})$ as discussed in Section II. We also test the Bessel function cusp correction proposed in Reference [26]. The coefficients $\{u_k\}$ and $\{p_{|\mathbf{G}|}\}$ are optimized in a variational Monte Carlo calculation, and then this optimized wavefunction is taken as the trial wavefunction for a DMC calculation to evaluate the ground state energy.

We use 4000 particle configurations in DMC, and by running tests with 2000, 4000, and 8000 configurations checked that 4000 configurations gives results within statistical uncertainty of the extrapolated result with an infinite number of configurations. Similarly we checked that our system of 81 particles gave similar results to systems of 45 and 145 particles, although a full extrapolation of results to the thermodynamic limit is not necessary to verify the accuracy of short ranged pseudopotentials, and so not a focus of this work. We did however correct the non-interacting energy of the system to the result of the infinite system, to reduce finite-size effects in the calculation [27, 48].

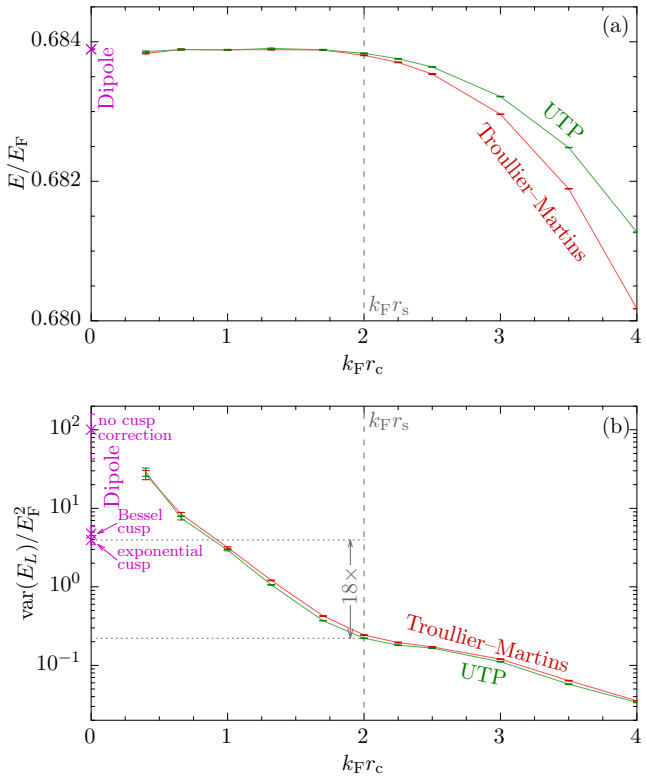

FIG. 5. (Color online) (a) The variation of the energy per particle in the Fermi gas with pseudopotential cutoff radius, calculated using DMC. The red points are for the Troullier–Martins pseudopotential, the green a UTP pseudopotential, and the magenta point is the exact dipolar potential. Stochastic error bars are of order $10^{-5}E_\mathrm{F}$. The vertical dashed line denotes the recommended cutoff radius. (b) The variance in the individual local energy samples (as seen in Fig. 1) taken during a DMC calculation using the pseudopotentials. Also shown are results for the dipolar potential both with and without Kato-like cusp corrections applied.

To evaluate the dipolar interaction we explicitly sum over pairs of particles within a distance R_s of each other, and then include the effect of particles further apart by integrating over them, assuming a uniform particle density. By taking R_s as ~ 18 simulation cell lattice vectors the error due to the finite value of R_s is smaller than $10^{-6}E_\mathrm{F}$, and therefore negligible compared to our DMC statistical errors [26, 49].

In order to analyze the accuracy of our pseudopotentials in capturing the dipolar gas, we start by fixing the

interaction strength and investigate the dependence of the accuracy on the cutoff radius r_c. Having selected a cutoff radius we then study the effect of the DMC timestep τ, and finally present results at a variety of interaction strengths.

In simulations using the pseudopotentials decreasing the cutoff radius makes the calculation more accurate by increasing the similarity to the real potential and reducing the likelihood of three-body interactions within the cutoff radius. This is shown in Fig. 5(a), calculated at $k_F r_0 = 1/2$ with timestep $\tau E_F = 0.0092$. However, this increased similarity to the dipolar potential also has the effect of increasing the variance in the individual local energy samples taken during the simulation, as shown in Fig. 5(b), which the runtime of a DMC calculation is proportional to [31]. When using the pseudopotentials a balance therefore has to be struck between accuracy and speedup: we choose to take the cutoff radius as equal to r_s, the density parameter that corresponds to the average separation of particles. This gives DMC calculations with an accuracy of order $10^{-4} E_F$, whilst as shown in Fig. 5(a) this accuracy quickly drops off for $r_c > r_s$.

In Fig. 5(b) we compare the variance in the individual local energy samples from the pseudopotentials to that from the real dipolar potential, using wavefunctions both with and without Kato-like cusp corrections applied. The two forms of cusp correction, the Bessel function cusp correction proposed for this system in Reference [26] and our simpler exponential cusp correction, agree to within statistical uncertainty. As discussed in Section II this is because both give rise to $r^{-5/2}$ divergences in the local energy, which are preferable to the higher variance in the local energy from the bare dipolar potential, which diverges as r^{-3}. The source of this divergence is, however, more transparent for the exponential cusp correction than the Bessel function cusp correction, and so we use the exponential form in the rest of our calculations.

Taking $r_c = r_s$ for the cutoff radius gives an 18-times reduction in the variance of the local energy samples of the many-body system using a pseudopotential when compared to using the real dipolar interaction with a Kato-like exponential cusp correction. To get the same statistical error in our results we therefore need to take 18 times fewer samples, leading to an 18-times statistical speedup in calculations.

There is however an additional speedup benefit from using the pseudopotential. The random walk in the DMC calculations is performed at a finite timestep τ [32, 50]. The use of a short-time approximation in the DMC algorithm gives rise to a linear dependence of the final estimate of the energy on τ [32]. If we were to use a short timestep to remove this systematic error the DMC walkers would not be able to move far in configuration space in each step, giving rise to serial correlations in the calculated values of the energy, and an explicit $\tau^{-1/2}$ dependence of the statistical standard error in the energy [51]. These two competing effects are shown in Fig. 6(a) and Fig. 6(b) respectively for our Fermi gas at $k_F r_0 = 1/2$.

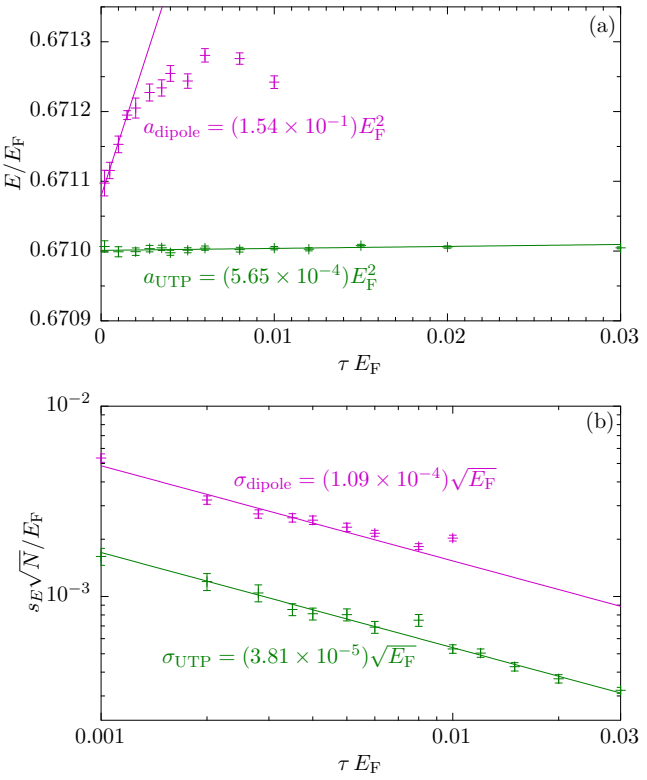

FIG. 6. (Color online) (a) The variation of the energy per particle in the Fermi gas with timestep τ. The magenta points are using the exact dipolar potential, and the green points using a UTP pseudopotential. The error bars show DMC stochastic errors, and are of order $10^{-5} E_F$. Fitted values of the linear error parameters a (see main text) are also given. (b) The standard error s_E in the energy per particle in the Fermi gas, for both the dipolar potential and UTP pseudopotential. Values of the fitting parameters σ for a $1/\sqrt{\tau}$ fit are also given for each.

The dependence on the energy on τ is both flatter when using the UTP compared to the dipolar potential, and also retains its linear form out to larger timesteps: this is advantageous as it allows the use of longer timesteps in DMC, which is more efficient. Fig. 6(b) confirms the $\tau^{-1/2}$ dependence of the standard error in the energy, and that the smoothness of the UTP delivers a smaller standard error.

We express the linear short-time approximation as giving an offset in the calculated energy of $a\tau$, where a is a fitting parameter, and the serial correlations as giving a variance in the energy of $s_E^2 = \sigma^2 N^{-1} \tau^{-1}$, with σ being a fitting parameter. The statistical error can be reduced by taking more samples N [31]. We can then express the expected value of the square error in the energy as being distributed to leading order as a Gaussian [28, 52]

$$\begin{aligned} \langle \Delta E^2 \rangle &= \int \Delta E^2 \mathrm{e}^{-\frac{(\Delta E - a\tau)^2}{2\sigma^2 N^{-1}\tau^{-1}}} \mathrm{d}(\Delta E) \\ &= a^2\tau^2 + \sigma^2 N^{-1} \tau^{-1}. \end{aligned} \tag{8}$$

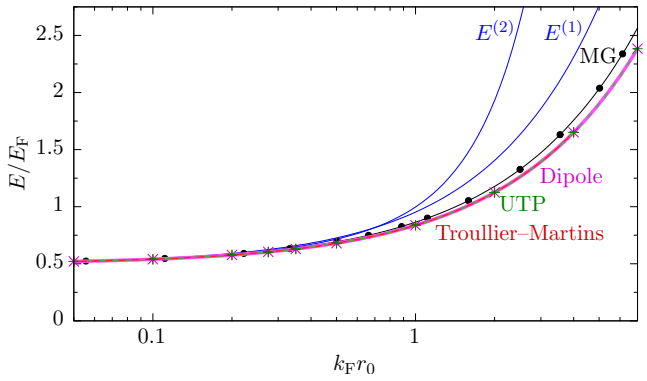

FIG. 7. (Color online) The equation of state of the 2D isotropic, homogeneous dipolar gas. The blue curves show the first- and second-order perturbation theory ($E^{(1)}$ and $E^{(2)}$) equations of state [42], and our DMC data are shown in: magenta, for the dipolar potential; red for the Troullier–Martins pseudopotential calibrated at $E_F/4$; and green for a UTP. The latter three curves overlie each other to within the width of the plotted lines. Stochastic error bars are of order $10^{-5}E_F$. The black circles show data from DMC calculations using the dipolar potential by Matveeva and Giorgini (MG) in Reference [26].

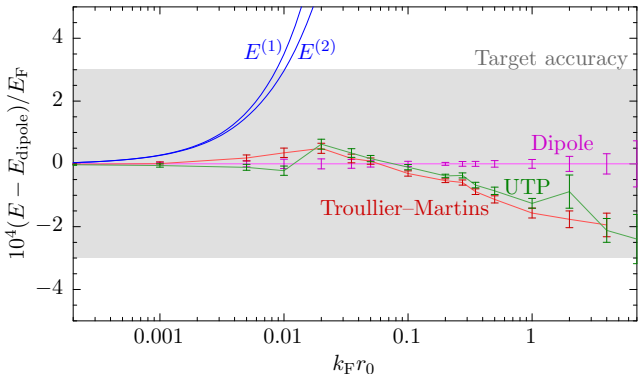

FIG. 8. (Color online) The deviation of the equation of state as calculated using the pseudopotentials from that calculated using the exact dipolar potential. The dipolar potential is shown in magenta, with the Troullier–Martins pseudopotential in red, the UTP in green, and first- and second-order perturbation theory ($E^{(1)}$ and $E^{(2)}$) in blue. The gray box around the results using the dipolar potential shows the target $3 \times 10^{-4}E_F$ accuracy level.

The expected square error in the energy is minimized at the optimal timestep

$$\tau_{\text{optimum}} = \left(\frac{1}{2}\frac{\sigma^2}{a^2}\frac{1}{N}\right)^{1/3},$$

and substituting this into Equation (8), the ratio of the number of steps required to give the same expected square error in the energy when using the dipolar potential and the UTP is

$$\frac{a_{\text{dipole}}\sigma^2_{\text{dipole}}}{a_{\text{UTP}}\sigma^2_{\text{UTP}}}. \tag{9}$$

For the values of the fitting parameters a and σ in Fig. 6 this gives a ratio of required number of steps and hence speedup when using the pseudopotential of ~ 2230. This value for the speedup includes the variance difference of 18 that was found with the recommended value of r_c, the remainder coming from the improvement of the finite timestep behavior when using the pseudopotential.

Use of a second order propagator in the DMC algorithm might improve the efficiency of the calculations by allowing the use of a longer timestep than was possible here [53–55]. In a second order DMC algorithm the square error in the energy would take the form $\langle \Delta E^2 \rangle = b^4\tau^4 + \sigma^2 N^{-1}\tau^{-1}$. The parameter b, which is zero if the exact wavefunction is used in DMC, should grow with the standard deviation in the local energy. This same effect is seen in Fig. 6(a) and in the results of Reference [28]. We therefore expect $b_{\text{UTP}} < b_{\text{dipole}}$, and saw above that $\sigma_{\text{UTP}} < \sigma_{\text{dipole}}$. With this form of the square error in the energy, the speedup when using the pseudopotential relative to the real dipolar potential would take the form $b_{\text{dipole}}\sigma^2_{\text{dipole}}/(b_{\text{UTP}}\sigma^2_{\text{UTP}})$. We obtain the same statistical speedup as in the linear case from the factor $\sigma^2_{\text{dipole}}/\sigma^2_{\text{UTP}}$, and the ratio $b_{\text{dipole}}/b_{\text{UTP}}$ should be greater than 1, as was found for the ratio $a_{\text{dipole}}/a_{\text{UTP}}$ in the linear case, to further increase the speedup.

Recognizing that our pseudopotential gives accurate results with around 2000-times smaller computational outlay than using the real dipolar interaction, we now investigate the third parameter that could affect the accuracy, interaction strength.

B. Equation of state

We compare the equations of state of the 2D dipolar Fermi gas as calculated using the exact dipolar potential and the Troullier–Martins and UTP pseudopotentials in Fig. 7. The pseudopotential cutoff is taken as $r_c = r_s$ and we extrapolate to zero timestep following the procedure outlined in Reference [50]. We find the equations of state to be the same to order $10^{-4}E_F$. Shown as black circles in Fig. 7 is the equation of state of the system as calculated using DMC by Matveeva and Giorgini (MG) in Reference [26]. We explicitly repeat the simulation of Reference [26], using the same system of 81 particles, but our calculated energies using the dipolar potential are of order $10^{-2}E_F$ lower than reported there, and as DMC is a variational technique this indicates that our trial wavefunction is likely more accurate than was available to the authors of Reference [26], possibly due to our inclusion of a Jastrow factor with variational parameters. On the scale of Fig. 7 it is not possible to distinguish our pseudopotential calculations from those using the real dipo-

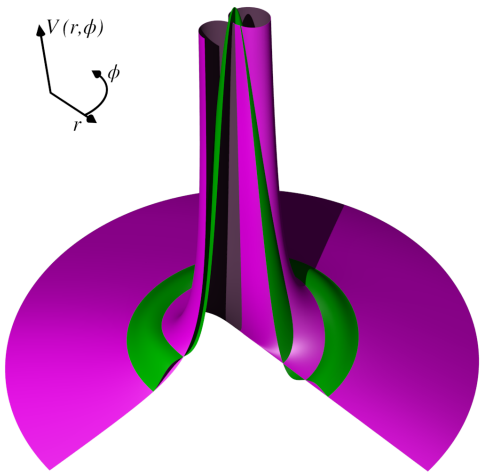

FIG. 9. (Color online) The dipolar potential $V(r,\phi)$ in magenta, and the UTP $V_{\rm UTP}(r,\phi)$ for the same tilt angle, in green. The potentials are cut through for $3\pi/2 < \phi < 2\pi$ to contrast the radial variation of the dipolar potential along $\phi = 3\pi/2$ and $\phi = 2\pi$, and show the smooth join of the UTP onto the dipolar potential at $r = r_{\rm c}$.

lar interaction, and so in order to properly analyze them we examine the error from the true dipolar potential in Fig. 8.

Following the accuracy used in Reference [26] to draw conclusions about which phases are energetically favorable in the dipolar gas, we choose a target accuracy of $3\times10^{-4}E_{\rm F}$ for our pseudopotentials, shown as a gray box in Fig. 8. Over a wide range of interaction strengths our pseudopotentials fall within this accuracy, with the UTP being slightly more accurate than the Troullier–Martins pseudopotential at most interaction strengths. We also compare our DMC results to second-order perturbation theory [42, 56]

$$E^{(2)} = \frac{E_{\rm F}}{2}\left[1 + \frac{128}{45\pi}k_{\rm F}r_0 + \frac{1}{4}(k_{\rm F}r_0)^2\ln(1.43k_{\rm F}r_0)\right],$$

noting that it differs significantly from the DMC results above interaction strengths of $k_{\rm F}r_0 \gtrsim 0.01$. In Fig. 7 we also note that above $k_{\rm F}r_0 \gtrsim 1$ first-order perturbation theory is more accurate than $E^{(2)}$, indicating that perturbation theory is not an adequate approximation except at very low interaction strengths $k_{\rm F}r_0 \ll 0.01$.

We have constructed and tested pseudopotentials using the Troullier–Martins and UTP methods. In each test, shown in Figures 3(b), 4, and 8, the UTP method has given more accurate results. We therefore recommend the use of the UTP method to construct pseudopotentials for the dipolar interaction, and recommend its use over the dipolar potential with a cusp correction due to the 2000-times speedup in calculations that can be achieved whilst still achieving sufficient accuracy. We now go on to show that the UTP can be generalized to capture the effects of an anisotropic interaction in a system of tilted dipoles.

VI. TILTED DIPOLES

The above analysis has focused on dipoles aligned normal to their 2D plane of motion by an external electric or magnetic field. However, this same electric or magnetic field could be used to align the dipoles at an angle θ to the normal to the plane [10]. The dipolar interaction then takes the anisotropic form $V(r,\phi) = d^2[1 - \frac{3}{2}\sin^2\theta(1+\cos 2\phi)]/r^3$ where ϕ is the polar angle in the plane, between the dipole-dipole separation and the projection of the electric field. We focus on the $\theta \le \theta_{\rm c} = \arcsin(1/\sqrt{3})$ regime, where the potential is purely repulsive and there are no bound states. The potential $V(r,\phi)$ is shown in magenta in Fig. 9 for $\theta = \theta_{\rm c}$ and $k_{\rm F}r_0 = 1/2$. As well as the r^{-3} divergence, the potential is strongly anisotropic, separating into two lobes. These properties make it difficult to work with numerically, and so we again develop a pseudopotential to ease the numerical simulation of this system.

The Troullier–Martins formalism used in the non-tilted system is not applicable to the case of $\theta > 0$, and so here we propose the UTP

$$V_{\rm UTP}(r,\phi) = \frac{d^2}{r_{\rm c}^3}\begin{cases} \left[1-\frac{3}{2}\sin^2\theta(1+\cos2\phi)\right] + 3\left(1-\frac{r}{r_{\rm c}}\right)\left(\frac{r}{r_{\rm c}}\right)^2\left[1-\frac{3}{2}\sin^2\theta(1+\cos2\phi)\right] \\ \quad + \left(1-\frac{r}{r_{\rm c}}\right)^2\left(1-\frac{3}{2}\sin^2\theta\right)\left[v_1\left(\frac{1}{2}+\frac{r}{r_{\rm c}}\right) + \sum_{i=2}^{N_v} v_i\left(\frac{r}{r_{\rm c}}\right)^i\right] \\ \quad + \sin^2\theta\cos2\phi\left[\left(1-\frac{r}{r_{\rm c}}\right)^2 v_{N_v+1}\left(\frac{r}{r_{\rm c}}\right)^2 + 3\left(\frac{1}{2}-\frac{3}{2}\left(\frac{r}{r_{\rm c}}\right)^2+\left(\frac{r}{r_{\rm c}}\right)^3\right)\right], & r < r_{\rm c}, \\ \left[1-\frac{3}{2}\sin^2\theta(1+\cos2\phi)\right] r_{\rm c}^3/r^3, & r \ge r_{\rm c}, \end{cases} \tag{10}$$

which is constrained to be smooth to first derivative in both radial and azimuthal directions at the origin and at $r_{\rm c}$, where it joins onto the exact dipolar potential. N_v is again set as 3, and the coefficients $\{v_i\}$ are minimized

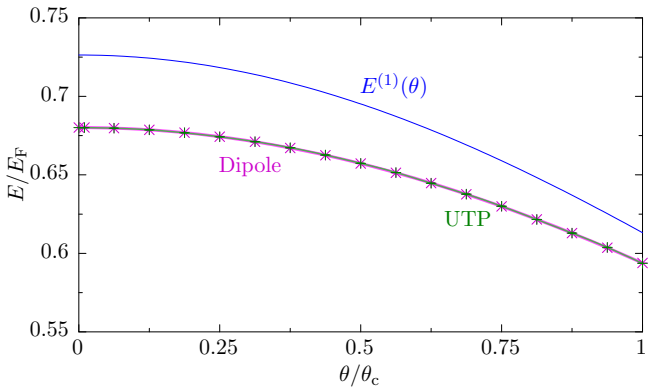

FIG. 10. (Color online) The equation of state of the tilted dipolar gas system as a function of tilt angle θ. Our DMC data using the dipolar potential and UTP overlie one another to within the width of the plotted lines, with stochastic error bars of order $10^{-5}E_F$. First-order perturbation theory $E^{(1)}$ is shown in blue.

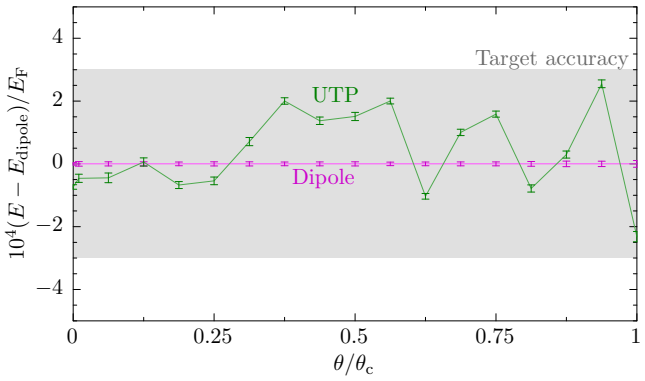

FIG. 11. (Color online) The deviation of the equation of state as calculated using the tilted pseudopotential from that calculated using the exact dipolar potential. Results using the dipolar potential are shown in magenta, with those using UTP pseudopotential in green. Similarly to Fig. 8, the gray box around the results using the dipolar potential shows the targeted $3 \times 10^{-4}E_F$ accuracy level.

similarly to the non-tilted case. At $\theta = 0$ Equation (10) reduces to the non-tilted form. A sample UTP is shown along with the tilted dipolar potential in Fig. 9, demonstrating its non-divergent properties at particle coalescence and that it smoothly merges into the dipolar potential at $r = r_c$. Furthermore, the angular variation of the UTP is less extreme than the real dipolar potential, which should lead to smoother estimates of the local energy at high tilt angles.

To optimize the pseudopotential we again calibrate in the two-body system. The $\cos 2\phi$ term in the potential couples together angular momentum channels of the wavefunction that differ by two angular momentum quanta, meaning that we can no longer solve the Schrödinger Equation separately in each angular momentum channel. Now that weight will be passed between the channels, they need to be considered explicitly and simultaneously.

We solve the Schrödinger Equation simultaneously in the lowest four occupied angular momentum channels, $\ell = \{1, 3, 5, 7\}$, numerically for both the dipolar potential and, separately, using the pseudopotential, in order to find values for the coefficients $\{v_i\}$. As part of this process we optimise the weight in each channel. Unlike in the $\theta = 0$ case it is not possible to find an analytic scattering wavefunction in the two-body homogeneous system that correctly captures the physics of the system in any limit. Instead we optimise the parameters $\{v_i\}$ by matching the energy of two particles in an harmonic trap, in effect minimising the error that was shown in Fig. 4.

We need to select an optimal trap frequency ω at which to calibrate the pseudopotential. To do this, we re-write the reduced system Hamiltonian for particles in an harmonic trap as $\hat{H} = \hat{H}_{iso}(\hat{r}) + \hat{H}_{aniso}(\hat{r}, \hat{\phi})$, with

$$\hat{H}_{iso}(\hat{r}) = -\nabla^2 + \frac{1}{4}\omega^2\hat{r}^2 + \frac{\bar{d}^2}{\hat{r}^3},$$
$$\hat{H}_{aniso}(\hat{r}, \hat{\phi}) = -\frac{\bar{d}^2}{\hat{r}^3}\frac{\frac{3}{2}\sin^2\theta}{1 - \frac{3}{2}\sin^2\theta}\cos 2\hat{\phi},$$

and $\bar{d}^2 = d^2(1 - \frac{3}{2}\sin^2\theta)$. $\hat{H}_{iso}$ captures the effect of the harmonic trap and the isotropic part of the dipolar interaction, whilst $\hat{H}_{aniso}$ captures the anisotropic part of the dipolar interaction. We seek a trap frequency ω at which the average kinetic energy of the harmonic trap system is the same as that of the homogenous system, allowing us to select the appropriate Fermi momentum k_F to describe the interaction strength $k_F r_0$. For the isotropic part of the Hamiltonian we can apply a cusp correction to the non-interacting harmonic trap wavefunction, in the same spirit as Section II. This gives a trial wavefunction

$$\psi(r, \phi) \propto \omega\, r\, e^{-\frac{1}{4}\omega r^2 - 2\frac{d}{\sqrt{r}}}.$$

We set the average kinetic energy of the isotropic harmonic trap system as equal to the kinetic energy of the homogeneous system and solve for ω, which for interaction strength $k_F r_0 = 1/2$ is $\omega_{iso} \approx 2.2E_F$.

Having analyzed the isotropic part of the Hamiltonian we now turn to the anisotropic $\hat{H}_{aniso}$. As there is no analytical solution to the tilted two-body scattering problem available we instead perform a perturbative analysis in small θ. We search for the most important contribution that $\hat{H}_{aniso}$ makes to the system's energy, which occurs where $|\psi(r, \phi)\hat{H}_{aniso}\psi(r, \phi)|$ is maximal. This is at $r \approx r_0$ and $\phi = 0$, and using these values in the functional form of $\hat{H}_{aniso}$ we get a perturbative energy $\frac{3}{2}r_0^{-2}\sin^2\theta\left(1 - \frac{9}{4}\sin^4\theta\right)$ for small θ. Adding this to the isotropic trap frequency we obtain the harmonic trap frequency $\omega \approx 2.2E_F + \frac{3}{2}r_0^{-2}\sin^2\theta\left(1 - \frac{9}{4}\sin^4\theta\right)$, which we

use to optimise the pseudopotentials. An example UTP is shown in Fig. 9, demonstrating its smooth and non-divergent properties. The form of the pseudopotential is robust against changes in the trap frequency ω used to construct it. With the pseudopotential in place we perform DMC calculations to evaluate the ground state energy of the anisotropic, homogeneous dipolar gas. In Fig. 10 we show the equation of state of the tilted dipole gas at interaction strength $k_{\mathrm{F}}r_0 = 1/2$ over a range of tilt angles $0 \leq \theta \leq \theta_{\mathrm{c}}$ away from vertical. We use a similar trial wavefunction to the non-tilted case, with the addition to the Jastrow factor of an anisotropic term

$$\prod_{i\neq j} \exp\left[\left(\sum_{k=0}^{N_{\mathrm{s}}} s_k r_{ij}^k \cos\left(2\phi_{ij}\right)\right)\left(1-\frac{r_{ij}}{L}\right)^3 \Theta(L-r_{ij})\right],$$

where the variables have the same meaning as in Equation (7), ϕ_{ij} is the polar angle between the particles labelled i, j, and $N_{\mathrm{s}} = 6$. This term captures the leading-order anisotropies in the inter-particle correlations. The addition of higher-order angular terms did not provide any significant benefit. In calculations using the real tilted dipolar potential we also modify the cusp condition to the form $\prod_{i>j} \exp(-2\bar{d}/\sqrt{r_{ij}})$.

In Fig. 10 we compare our DMC estimates of the equation of state to first-order perturbation theory [13]

$$E^{(1)}(\theta) = \frac{E_{\mathrm{F}}}{2}\left[1 + \frac{128}{45\pi}k_{\mathrm{F}}r_0\left(1-\frac{3}{2}\sin^2\theta\right)\right].$$

Similarly to the non-tilted case we find that perturbation theory overestimates the energy, and also that it overestimates the reduction in energy with increasing tilt angle. Again the results using the exact dipolar interaction and those using our UTP are so similar they cannot be distinguished on this scale, and so we analyze the pseudopotential accuracy by examining the energy error from the dipolar potential in Fig. 11. As in the non-tilted system the pseudopotential achieves our target accuracy of $3\times10^{-4}E_{\mathrm{F}}$ across a wide range of parameter space. The pseudopotential is particularly accurate below $\theta \lesssim \theta_{\mathrm{c}}/4$ where there is less coupling between angular momentum channels, at $\theta \to 0$ reproducing the same accuracy that was found in the non-tilted system.

To determine the full benefit of using the pseudopotential in a tilted system we examine the behavior of the calculated energy with DMC timestep in Fig. 12, evaluated at $k_{\mathrm{F}}r_0 = 1/2$ and $\theta = \theta_c/2$. Similarly to the non-tilted case, Fig. 12(a) shows that the energy calculated using the pseudopotential has significantly improved behavior with timestep when compared to the dipolar potential, having less severe variation of the energy with timestep and also remaining in the linear regime out to larger τ. There is also a reduction in standard error of ~ 2.2 times when using the pseudopotential, as seen in Fig. 12(b). Combining the fitting parameters in Fig. 12 in the way set out in Section V A shows the pseudopotential to be $\sim$ 450 times quicker to use than the real tilted dipolar interaction.

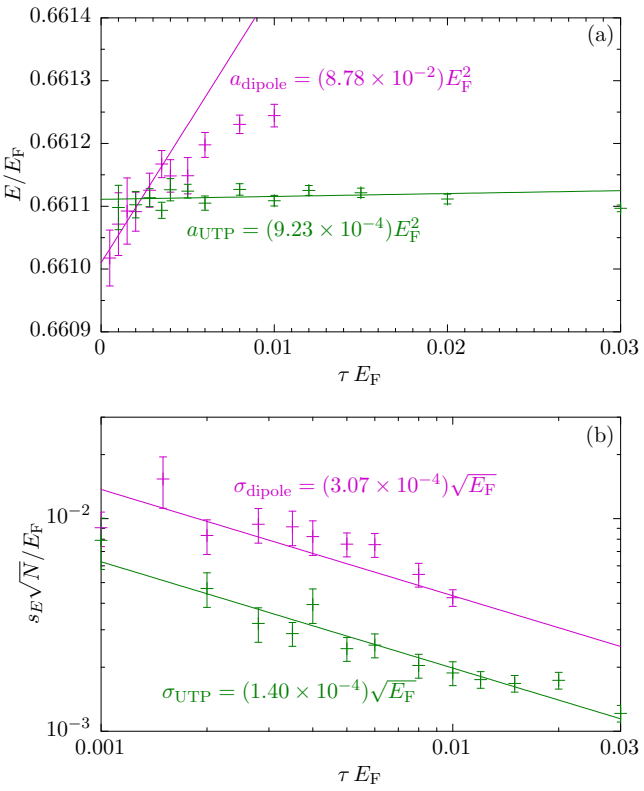

FIG. 12. (Color online) (a) The variation of the energy per particle in the Fermi gas of tilted dipoles with timestep τ, with the values of the linear error parameters a. (b) The standard error s_{E} in the energy per particle in the Fermi gas, again with fitted $1/\tau$ parameters given.

We have constructed pseudopotentials for the dipolar interaction at tilt angles $0 \leq \theta \leq \theta_{\mathrm{c}}$, and shown that they give the ground state energy of the anisotropic, homogeneous dipolar gas to within $3\times10^{-4}E_{\mathrm{F}}$, and also provide a 450-times speedup over using the real tilted dipolar interaction. This means that they will be an accurate and efficacious tool to carry out DMC investigations of the whole $0 \leq \theta \leq \theta_{\mathrm{c}}$ phase diagram.

VII. DISCUSSION

We have developed accurate pseudopotentials for the dipolar interaction in two dimensions and tested them against the dipolar interaction by comparing scattering phase shifts, energies in an harmonic trap, and the ground state of a Fermi gas. The pseudopotentials deliver ground state energies of the Fermi gas to an accuracy of $3\times10^{-4}E_{\mathrm{F}}$, and their smoothness accelerates DMC calculations by a factor of up to ~ 2000.

The pseudopotentials have been constructed to work in situations where the dipole moments are aligned both normal and at an angle to the two-dimensional plane of motion of the particles. This could allow the formal-

ism developed here to be used in an analysis of the full phase diagram of the 2D dipolar gas, including investigating the high interaction strength regime where the Fermi fluid forms a Wigner-type crystal [26], possibly after passing through a stripe phase [13], or to turn to the tilted section of the phase diagram, with the possibility of superfluid behavior at high tilt angles [57]. Superfluidity is also expected in a system of dipoles dressed by an external microwave field [58, 59], a system that would also be amenable to analysis using a pseudopotential. The method used here for constructing pseudopotentials for the tilted system could also be extended to a 3D system of dipolar particles, or to study a classical analogue of the system.

ACKNOWLEDGMENTS

The authors thank Pascal Bugnion, Neil Drummond, Pablo López Ríos, and Richard Needs for useful discussions. TMW acknowledges the financial support of the EPSRC [EP/J017639/1], and GJC acknowledges the financial support of the Royal Society and Gonville & Caius College. There is Open Access to this paper and data available at `https://www.repository.cam.ac.uk`.

Appendix A: Construction of the Troullier–Martins pseudopotentials

The Troullier–Martins formalism is a method for developing pseudopotentials that were originally designed for use in electron-ion calculations [35]. Here, following Reference [27] we adapt it to the case of a 2D dipolar potential. The scattering Schrödinger Equation (1) may be written in 2D circular coordinates (r, ϕ) as

$$-\left(\frac{1}{r}\frac{\partial}{\partial r}\left(r\frac{\partial}{\partial r}\right)+\frac{1}{r^2}\frac{\partial^2}{\partial\phi^2}\right)\psi(r,\phi)+V(r)\psi(r,\phi) = E\psi(r,\phi)\,,$$

where we wish to replace the dipolar potential $V(r) = d^2/r^3$ with a pseudopotential inside a cutoff radius r_c. Expanding the wavefunction in angular momentum channels as

$$\psi(r,\phi)=\sum_{\ell=0}^{\infty} r^\ell \psi_\ell(r)\cos(\ell\phi)$$

we obtain a radial equation for the wavefunction ψ_ℓ in each channel

$$-\left(\frac{2\ell+1}{r}\psi'_\ell+\psi''_\ell\right)+V(r)\psi_\ell = E\psi_\ell\,, \tag{A1}$$

where the primes indicate differentiation with respect to r. We choose a calibration energy E_c at which the pseudopotential will exactly replicate the dipolar potential's scattering characteristics, whose optimal choice is found in Appendix B to be $E_\mathrm{F}/4$. We then construct the pseudopotential by working from a pseudo-wavefunction that within a radius r_c takes the form

$$\psi_{\mathrm{pseudo},\ell}(r) = \mathrm{e}^{p(r)}\,,$$

where $p(r)=\sum_{i=0}^{6} c_i r^{2i}$. The form $\mathrm{e}^{p(r)}$ is positive definite, which ensures that no spurious nodes are introduced into the wavefunction. Inserting the wavefunction into Equation (A1) we find that the pseudopotential in each angular momentum channel ℓ should take the form

$$V_{\mathrm{T\text{–}M}}(r)=\begin{cases} E_\mathrm{c}+\frac{2\ell+1}{r}p'+p'^2+p'', & r<r_\mathrm{c},\\ d^2/r^3, & r\geq r_\mathrm{c}\,. \end{cases} \tag{A2}$$

In order to calculate $p(r)$ explicitly we impose a series of constraints on it: firstly, that the pseudo-wavefunction's value and first four derivatives match those of the exact wavefunction at r_c, in order that the first two derivatives of the pseudopotential are continuous,

$$\begin{aligned}
p(r_\mathrm{c}) &= \ln\left(\frac{R_\ell(r_\mathrm{c})}{r_\mathrm{c}^{\ell+1}}\right),\\
p'(r_\mathrm{c}) &= \frac{R'_\ell(r_\mathrm{c})}{R_\ell(r_\mathrm{c})}-\frac{\ell+1}{r_\mathrm{c}},\\
p''(r_\mathrm{c}) &= V(r_\mathrm{c})-E_\mathrm{c}-(p'(r_\mathrm{c}))^2-\frac{2\ell+1}{r_\mathrm{c}}p'(r_\mathrm{c}),\\
p'''(r_\mathrm{c}) &= V'(r_\mathrm{c})-2p'(r_\mathrm{c})p''(r_\mathrm{c})-\frac{2\ell+1}{r_\mathrm{c}}p''(r_\mathrm{c})\\
&\quad+\frac{2\ell+1}{r_\mathrm{c}^2}p'(r_\mathrm{c}),\\
p''''(r_\mathrm{c}) &= V''(r_\mathrm{c})-2(p''(r_\mathrm{c}))^2-2p'(r_\mathrm{c})p'''(r_\mathrm{c})\\
&\quad-\frac{2\ell+1}{r_\mathrm{c}}p'''(r_\mathrm{c})+2\frac{2\ell+1}{r_\mathrm{c}^2}p''(r_\mathrm{c})-2\frac{2\ell+1}{r_\mathrm{c}^3}p'(r_\mathrm{c}),
\end{aligned}$$

where $R_\ell(r) = r\psi_{\mathrm{dipole},\ell}(r)$. The polynomial form of $p(r)$ ensures that this is a set of linear equations in the coefficients c_i, and so has a straighforward solution. We also require that the pseudo-wavefunction has zero curvature at the origin,

$$c_2^2 = -c_4(2\ell+4),$$

and that the norm of the pseudo-wavefunction within the cutoff radius is the same as that from the exact potential, to conserve the physical particle weight

$$\begin{aligned}
&2c_0+\ln\left(\int_0^{r_\mathrm{c}} r^{2\ell+1}\exp\left(2p(r)-2c_0\right)\mathrm{d}r\right)\\
&\qquad=\ln\left(\int_0^{r_\mathrm{c}}|\psi_{\mathrm{dipole},\ell}(r,\phi)|^2 r\mathrm{d}r\right).
\end{aligned}$$

This fully specifies $p(r)$ and hence, via Equation (A2), $V_{\mathrm{T\text{–}M}}$. We solve these equations simultaneoulsy for the c_i, always taking the branch of the quadratic equation that gives the smaller value for c_0, which in turn gives a larger reduction in variance for simulations using the pseudopotential.

Appendix B: Choosing a calibration energy

The Troullier–Martins formalism for deriving pseudopotentials is designed to give exact scattering properties at the calibration energy. The norm-conservation condition may also be considered as requiring that the derivative of the phase shift with respect to energy evaluated at the calibration energy $\partial\Delta\delta/\partial E|_{E_c} = 0$ [27]. This means that to leading order the error in the scattering phase shift when using a Troullier–Martins pseudopotential $\Delta\delta \propto (E - E_c)^2$. Expressing this in terms of the relative momentum $\mathbf{k}_1 - \mathbf{k}_2$ of the two scattering particles with momenta $\mathbf{k}_1$, $\mathbf{k}_2$, the scattering phase shift error $\Delta\delta(|(\mathbf{k}_1 - \mathbf{k}_2)/2|^2) \propto (|(\mathbf{k}_1 - \mathbf{k}_2)/2|^2 - k_c^2)^2$ where $k_c = \sqrt{E_c}$ is the calibration wave vector. To find the optimum calibration wave vector we average this error over the Fermi sea for particles 1 and 2 and then minimize with respect to k_c. The average

$$\langle\Delta\delta\rangle = \frac{\int \Delta\delta\left(\left|\frac{\mathbf{k}_1 - \mathbf{k}_2}{2}\right|^2\right) n(k_1)n(k_2)\,\mathrm{d}\mathbf{k}_1\,\mathrm{d}\mathbf{k}_2}{\int n(k_1)n(k_2)\,\mathrm{d}\mathbf{k}_1\,\mathrm{d}\mathbf{k}_2}, \quad \text{(B1)}$$

where $n(k)$ is the Fermi-Dirac distribution, can be rewritten in terms of center-of-momentum and relative coordinates $\mathbf{x} = (\mathbf{k}_1 - \mathbf{k}_2)/2k_F$, $\mathbf{y} = (\mathbf{k}_1 + \mathbf{k}_2)/2k_F$, which transforms Equation (B1) into [42]

$$\langle\Delta\delta\rangle \propto \int_0^{2\pi}\int_0^1\int_0^{y_0(x,\phi)} \Delta\delta(k_F^2x^2)\,x\,y\,\mathrm{d}y\,\mathrm{d}x\,\mathrm{d}\phi\,,$$

where ϕ is the angle between $\mathbf{x}$ and $\mathbf{y}$ and the function $y_0(x,\phi) = -x|\cos\phi| + \sqrt{1 - x^2\sin^2\phi}$. This then simplifies to

$$\langle\Delta\delta\rangle \propto \int_0^1 x\Delta\delta(k_F^2x^2)\left(\pi - 2\left(x\sqrt{1-x^2} + \arcsin x\right)\right)\mathrm{d}x\,,$$

and substituting the form of $\Delta\delta \propto (k_F^2x^2 - k_c^2)^2$ from above the optimum value of k_c is found to be $k_F/2$, and hence the optimum calibration energy $E_c = E_F/4$.

[1] C.-H. Wu, J.W. Park, P. Ahmadi, S. Will, and M.W. Zwierlein, Phys. Rev. Lett. **109**, 085301 (2012)
[2] J. Werner, A. Griesmaier, S. Hensler, J. Stuhler, T. Pfau, A. Simoni, and E. Tiesinga, Phys. Rev. Lett. **94**, 183201 (2005)
[3] T. Lahaye, T. Koch, B. Fröhlich, M. Fattori, J. Metz, A. Griesmaier, S. Giovanazzi, and T. Pfau, Nature **448**, 672 (2007)
[4] B. Neyenhuis, B. Yan, S.A. Moses, J.P. Covey, A. Chotia, A. Petrov, S. Kotochigova, J. Ye, and D.S. Jin, Phys. Rev. Lett. **109**, 230403 (2012)
[5] J.W. Park, S.A. Will, and M.W. Zwierlein, Phys. Rev. Lett. **114**, 205302 (2015)
[6] D. Wang, B. Neyenhuis, M.H.G. de Miranda, K.-K. Ni, S. Ospelkaus, D.S. Jin, and J. Ye, Phys. Rev. A **81**,061404 (2010)
[7] T. Takekoshi, L. Reichsöllner, A. Schindewolf, J.M. Hutson, C.R. Le Sueur, O. Dulieu, F. Ferlaino, R. Grimm, and H.C. Nägerl, Phys. Rev. Lett. **113**, 205301 (2014)
[8] K.-K. Ni, S. Ospelkaus, M.H.G. de Miranda, A. Pe'er, B. Neyenhuis, J.J. Zirbel, S. Kotochigova, P.S. Julienne, D.S. Jin, and J. Ye, Science **322**, 231 (2008)
[9] G. Bismut, B. Laburthe-Tolra, E. Maréchal, P. Pedri, O. Gorceix, and L. Vernac, Phys. Rev. Lett. **109**, 155302 (2012)
[10] K.-K. Ni, S. Ospelkaus, D. Wang, G. Quéméner, B. Neyenhuis, M.H.G. de Miranda, J.L. Bohn, J. Ye, and D.S. Jin, Nature **464**, 1324 (2010)
[11] K. Aikawa, A. Frisch, M. Mark, S. Baier, R. Grimm, J.L. Bohn, D.S. Jin, G.M. Bruun, and F. Ferlaino, Phys. Rev. Lett. **113**, 263201 (2014)
[12] F. Cinti, P. Jain, M. Boninsegni, A. Micheli, P. Zoller, and G. Pupillo, Phys. Rev. Lett. **105**, 135301 (2010)
[13] M.M. Parish and F.M. Marchetti, Phys. Rev. Lett. **108**, 145304 (2012)
[14] G.E. Astrakharchik, J. Boronat, J. Casulleras, I.L. Kurbakov, and Yu.E. Lozovik, Phys. Rev. A **75**, 063630 (2007)
[15] F. Mazzanti, R.E. Zillich, G.E. Astrakharchik, and J. Boronat, Phys. Rev. Lett. **102**, 110405 (2009)
[16] A. Macia, F. Mazzanti, J. Boronat, and R.E. Zillich, Phys. Rev. A **84**, 033625 (2011)
[17] A. Macia, D. Hufnagl, F. Mazzanti, J. Boronat, and R.E. Zillich, Phys. Rev. Lett. **109**, 235307 (2012)
[18] A. Macia, G.E. Astrakharchik, F. Mazzanti, S. Giorgini, and J. Boronat, Phys. Rev. A **90**, 043623 (2014)
[19] A. Macia, J. Boronat, and F. Mazzanti, Phys. Rev. A **90**, 061601(R) (2014)
[20] N. Matveeva and S. Giorgini, Phys. Rev. Lett. **111**, 220405 (2013)
[21] N. Matveeva and S. Giorgini, Phys. Rev. A **90**, 053620 (2014)
[22] K.R.A. Hazzard, B. Gadway, M. Foss-Feig, B. Yan, S.A. Moses, J.P. Covey, N.Y. Yao, M.D. Lukin, J. Ye, D.S. Jin, and A.M. Rey, Phys. Rev. Lett. **113**, 195302 (2014)
[23] M.H.G. de Miranda, A. Chotia, B. Neyenhuis, D. Wang, G. Quéméner, S. Ospelkaus, J.L. Bohn, J. Ye, D.S. Jin, Nature Physics **7**, 502 (2011)
[24] Y. Yamaguchi, T. Sogo, T. Ito, and T. Miyakawa, Phys. Rev. A **82**, 013643 (2010)
[25] K. Sun, C. Wu, and S. Das Sarma, Phys. Rev. B **82**, 075105 (2010)
[26] N. Matveeva and S. Giorgini, Phys. Rev. Lett. **109**, 200401 (2012)

[27] P.O. Bugnion, P. López Ríos, R.J. Needs, and G.J. Conduit, Phys. Rev. A **90**, 033626 (2014)

[28] J.H. Lloyd-Williams, R.J. Needs and G.J. Conduit, Phys. Rev. B **92**, 075106 (2015)

[29] C.D. Sherrill and H.F. Schaefer III, Adv. Quant. Chem. bf 34, 143 (1999)

[30] R.J. Bartlett and M. Musiał, Rev. Mod. Phys. **79**, 291 (2007)

[31] W.M.C. Foulkes, L. Mitas, R.J. Needs, and G. Rajagopal, Rev. Mod. Phys. **73**, 33 (2001)

[32] R.J. Needs, M.D. Towler, N.D. Drummond, and P. López Ríos, J. Phys.:Condens. Matter **22**, 023201 (2010)

[33] T. Kato, Commun. Pure and Appl. Math. **10** (2), 151 (1957)

[34] R.T. Pack and W.B. Brown, J. Chem. Phys. **45**, 556 (1966)

[35] N. Troullier and J.L. Martins, Phys. Rev. B **43**, 1993 (1991).

[36] J.R. Trail and R.J. Needs, J. Chem. Phys. **122**, 174109 (2005)

[37] J.R. Trail and R.J. Needs, J. Chem. Phys. **122**, 014112 (2005)

[38] V. Heine, Solid State Physics **24**, 1 (1970)

[39] D.R. Hamann, M. Schlüter, and C. Chiang, Phys. Rev. Lett. **43**, 1494 (1979).

[40] A. Zunger and M.L. Cohen, Phys. Rev. B **20**, 4082 (1979).

[41] G.B. Bachelet, D.R. Hamann, and M. Schlüter, Phys. Rev. B **26**, 4199 (1982).

[42] Z.K. Lu and G.V. Shlyapnikov, Phys. Rev. A **85**, 023614 (2012)

[43] S. Murmann, A. Bergschneider, V.M. Klinkhamer, G. Zürn, T. Lompe, S. Jochim, Phys. Rev. Lett. **114**, 080402 (2015)

[44] S.A. Moses, J.P. Covey, M.T. Miecnikowski, B. Yan, B. Gadway, J. Ye, and D.S. Jin, Science **350**, 659 (2015)

[45] P.O. Bugnion and G.J. Conduit, Phys. Rev. A **87**, 060502(R) (2013)

[46] G.J. Conduit, A.G. Green, and B.D. Simons, Phys. Rev. Lett. **103**, 207201 (2009)

[47] P. López Ríos, P. Seth, N.D. Drummond, and R.J. Needs, Phys. Rev. E **86**, 036703 (2012)

[48] S. Pilati, G. Bertaina, S. Giorgini, and M. Troyer, Phys. Rev. Lett. **105**, 030405 (2010)

[49] N.D. Drummond, N.R. Cooper, R.J. Needs, and G.V. Shlyapnikov, Phys. Rev. B **83**, 195429 (2011)

[50] R.M. Lee, G.J. Conduit, N. Nemec, P. López Ríos, and N.D. Drummond, Phys. Rev. E **83**, 066706 (2011)

[51] S.M. Rothstein and J. Vrbik, Journal of Computational Physics, **74**, 127 (1988)

[52] J.R. Trail, Phys. Rev. E **77**, 016703 (2008)

[53] M. Mella, G. Morosi, and D. Bressanini, Phys. Rev. E **61**, 2050 (2000)

[54] A. Sarsa, J. Boronat, and J. Casulleras, J. Chem. Phys. **116**, 5956 (2002)

[55] S. Chiesa, M. Mella, G. Morosi, and D. Bressanini, J. Chem. Phys. **119**, 5601 (2003)

[56] C.K. Chan, C. Wu, W.C. Lee, and S. Das Sarma, Phys. Rev. A **81**, 023602 (2010)

[57] G.M. Bruun and E. Taylor, Phys. Rev. Lett. **101**, 245301 (2008)

[58] N.R. Cooper and G.V. Shlyapnikov, Phys. Rev. Lett. **103**, 155302 (2009)

[59] J. Levinsen, N.R. Cooper, and G.V. Shlyapnikov, Phys. Rev. A **84**, 013603 (2011)